

Article

Stimulated Raman Scattering in $\text{Pb}(\text{MoO}_4)_{1-x}(\text{WO}_4)_x$ with $x = 0, 0.5, 0.8$ and 1.0 with Combined Frequency Shifts on High- and Low-Frequency Raman Modes under Synchronous Picosecond Laser Pumping

Milan Frank ^{1,*}, Sergei N. Smetanin ², Michal Jelínek ¹, David Vyhlídal ¹, Miron B. Kosmyna ³, Alexey N. Shekhovstov ³, Ksenia A. Gubina ², Vladislav E. Shukshin ², Petr G. Zverev ² and Václav Kubeček ¹

¹ Faculty of Nuclear Sciences and Physical Engineering, Czech Technical University, Břehová 7, 11519 Prague, Czech Republic; michal.jelinek@jfifi.cvut.cz (M.J.); david.vyhlidal@jfifi.cvut.cz (D.V.); vaclav.kubecek@jfifi.cvut.cz (V.K.)

² Prokhorov General Physics Institute of the Russian Academy of Sciences, Vavilova 38, 119991 Moscow, Russia; ssmetanin@bk.ru (S.N.S.); axiniy@list.ru (K.A.G.); shukshinve@lst.gpi.ru (V.E.S.); zverev@lst.gpi.ru (P.G.Z.)

³ State Scientific Institution, Institute for Single Crystals of National Academy of Sciences of Ukraine, Nauky Ave. 60, 61000 Kharkiv, Ukraine; kosmyna@isc.kharkov.ua (M.B.K.); shekhov@isc.kharkov.ua (A.N.S.)

* Correspondence: frankmil@jfifi.cvut.cz; Tel.: +420-2243-58671



Citation: Frank, M.; Smetanin, S.N.; Jelínek, M.; Vyhlídal, D.; Kosmyna, M.B.; Shekhovstov, A.N.; Gubina, K.A.; Shukshin, V.E.; Zverev, P.G.; Kubeček, V. Stimulated Raman Scattering in $\text{Pb}(\text{MoO}_4)_{1-x}(\text{WO}_4)_x$ with $x = 0, 0.5, 0.8$ and 1.0 with Combined Frequency Shifts on High- and Low-Frequency Raman Modes under Synchronous Picosecond Laser Pumping. *Crystals* **2022**, *12*, 148. <https://doi.org/10.3390/cryst12020148>

Academic Editor: Carlo Vicario

Received: 25 December 2021

Accepted: 18 January 2022

Published: 21 January 2022

Publisher's Note: MDPI stays neutral with regard to jurisdictional claims in published maps and institutional affiliations.



Copyright: © 2022 by the authors. Licensee MDPI, Basel, Switzerland. This article is an open access article distributed under the terms and conditions of the Creative Commons Attribution (CC BY) license (<https://creativecommons.org/licenses/by/4.0/>).

Abstract: Comparative characteristics of spontaneous and stimulated Raman scattering in $\text{Pb}(\text{MoO}_4)_{1-x}(\text{WO}_4)_x$ single crystals ($x = 0, 0.5, 0.8$, and 1.0) including both the high (ν_1) and low (ν_2) frequency internal anionic group vibrations have been investigated. It was found that among these crystals, $\text{Pb}(\text{MoO}_4)_{0.2}(\text{WO}_4)_{0.8}$ is the most suitable for multi-wavelength Raman laser in several Raman modes simultaneously. This is caused by the optimal relative Mo/W content corresponding to the most efficient coherent combination of the $(\text{MoO}_4)^{2-}$ and $(\text{WO}_4)^{2-}$ vibrations enhancing the output radiation characteristics of the synchronously pumped $\text{Pb}(\text{MoO}_4)_{0.2}(\text{WO}_4)_{0.8}$ Raman laser. Oscillation of up to twelve, closely spaced SRS components in a range of 1128–1360 nm and the strongest pulse shortening down to 1.16 ps in comparison with not only PbMoO_4 and PbWO_4 but also with all the earlier investigated nominally pure scheelite-like tungstate and molybdate crystals has been achieved.

Keywords: Raman laser; synchronous pumping; multi-wavelengths generation; pulse shortening; PbMoO_4 and PbWO_4 crystals and solid solutions

1. Introduction

Interest in scheelite-type PbMoO_4 and PbWO_4 crystals first appeared in the 1960s after work was published considering them to be promising optical materials for acousto-optics [1]. Later, these crystals were recognized as very efficient for many applications due to their unique properties. PbMoO_4 —in acousto-optical modulators, deflectors and phase shifters [2]; PbWO_4 —in electromagnetic detectors in high-energy accelerators used for high-energy physics research at CERN [3]; PbMoO_4 and PbWO_4 —in a scintillation (cryogenic) detector for rare event and dark matter searches [4]. In addition, PbMoO_4 and PbWO_4 are prospective active materials for Raman lasers including the crystals self-activated by rare earth laser ions [5–10]. In the Raman laser applications the most intense ν_1 Raman mode of these crystals was used for the laser radiation frequency shifts in stimulated Raman scattering (SRS). This Raman mode corresponds to totally symmetric stretching vibration of the $(\text{MoO}_4)^{2-}$ or $(\text{WO}_4)^{2-}$ tetrahedron anionic groups with the frequency of $\nu_1 = 870$ or 905 cm^{-1} , respectively [11]. Using high-Q optical cavity for the Raman-active crystal can help to obtain SRS conversion in crystals not only on the most intense ν_1 Raman mode but also on lower intense Raman modes [12–15]. It is also necessary to note that in

scheelite-type crystals the anionic group bending vibration ν_2 is a coherent combination of two twisting ($A_g + B_g$) and one scissoring Raman mode having a one-mode behavior. The ν_2 line is significantly wider than the ν_1 line [16]. This allowed to achieve radiation pulse shortening down to the inverse width of the widest ν_2 line in transient SRS with combined ($\nu_1 + \nu_2$) frequency shifts in the scheelite-type crystal series under synchronous pumping by repetitive picosecond laser pulses [17–19].

Study of solid solutions of related functional crystals with variable composition is of interest due to the possibility of fine control of structure and, in turn, physical parameters of the material and its functionality. The initial aim of mixing the PbMoO_4 and PbWO_4 crystals was to combine reasonable mechanical properties of PbMoO_4 with better optical transmission of PbWO_4 at short wavelengths [20]. A remarkable property of $\text{Pb}(\text{MoO}_4)_{1-x}(\text{WO}_4)_x$ solid solutions is that they crystallize as single crystals in the entire compositional range [20–23]. This property is important for optical applications especially in optoelectronics [2]. Investigation of Raman spectra of $\text{Pb}(\text{MoO}_4)_{1-x}(\text{WO}_4)_x$ mixed crystals showed that they have two-modes behaviour for the high-frequency (ν_1) stretching vibrations of the anionic groups (corresponding to the molybdate and tungstate anionic groups) but one-mode behaviour for the low-frequency (ν_2) bending vibrations of the anionic groups [21]. Therefore, optimization of the $\text{Pb}(\text{MoO}_4)_{1-x}(\text{WO}_4)_x$ composition can help to equalize contributions of the high-frequency ν_1 modes corresponding to molybdate and tungstate structures for efficient closely spaced double wavelength SRS generation. Additionally, it can help to artificially construct the widest and highest ν_2 line as a coherent combination of the $(\text{MoO}_4)^{2-}$ and $(\text{WO}_4)^{2-}$ anionic group bending Raman modes similarly to the natural $A_g + B_g$ mode combination in the bending ν_2 Raman line for radiation pulse shortening in ($\nu_1 + \nu_2$)-shifted SRS under synchronous picosecond pumping. The first observation of SRS in the $\text{Pb}(\text{MoO}_4)_{1-x}(\text{WO}_4)_x$ mixed crystal at $x = 0.5$ was carried out in work [24]. It was found that single-pass SRS conversion took place with the high-frequency shifts of $\nu_1 = 870$ and 905 cm^{-1} from the $\lambda_p = 1064 \text{ nm}$ pump wave into the first-order Stokes SRS doublet at $\lambda_s = (\lambda_p^{-1} - \nu_1)^{-1} = 1173$ and 1178 nm , but higher order SRS conversion was inefficient due to stronger splitting of the SRS radiation components.

In the present work, we have focused on multiwavelength combined shift SRS generation and the strongest pulse shortening. We have carried out a comparative study of synchronously pumped SRS in $\text{Pb}(\text{MoO}_4)_{1-x}(\text{WO}_4)_x$ single crystals with various content ratio of $x = 0, 0.5, 0.8$, and 1.0 . The optimum content ratio ($x = 0.8$) has been found for generation of the highest number (up to 12) of closely spaced wavelengths and the strongest pulse shortening (down to 1.16 ps) which is stronger than in nominally pure PbMoO_4 and PbWO_4 crystals (1.33 and 1.27 ps). The lasers generating at two or more wavelengths simultaneously are widely used in atmospheric detection, lidar system, and terahertz wave generation [25–27].

2. Raman Crystals Characterization

PbMoO_4 and PbWO_4 crystals are different from other scheelite-type crystals (alkali-earth tungstate and molybdate crystals) by a comparatively large degree of covalence of the bond between the cation (Pb^{2+}) and oxygen due to a comparatively large mass and electronegativity of the Pb^{2+} cation. This leads to an influence on the internal vibrations of anionic groups reducing the effective mass of the oscillating Mo-O or W-O pair in the anionic group [11]. We assumed that this effect is different for the molybdate and tungstate crystals, and therefore it would be interesting to control this effect in the mixed crystal.

For comparative investigation we used four samples: the a-cut PbMoO_4 (Nanjing Metalaser Photonics Co., Ltd., Nanjing, China) and PbWO_4 (Crytur, Ltd., Turnov, Czech Republic) crystal samples with equal lengths of 25 mm ; the a-cut $\text{Pb}(\text{MoO}_4)_{0.5}(\text{WO}_4)_{0.5}$ and $\text{Pb}(\text{MoO}_4)_{0.2}(\text{WO}_4)_{0.8}$ samples (State Scientific Institution “Institute for Single Crystals” of National Academy of Sciences of Ukraine, Kharkiv, Ukraine) with equal length of 14 mm . As for the mixed-crystals growth, dried initial components PbO (99.99%), WO_3 (99.99%), and MoO_3 (99.99%) were taken in the stoichiometric ratio and carefully mixed for synthesis

of $\text{PbWO}_4 + \text{PbMoO}_4$ compounds, respectively. To produce $\text{PbWO}_4 + \text{PbMoO}_4$ compounds, a solid-state synthesis was carried out for 6 h at 700 °C and 650 °C, respectively. Formation of the compounds took place according to the following reaction:



The growth of $\text{PbWO}_4 + \text{PbMoO}_4$ single crystals was carried out by the Czochralski method with a seed in argon atmosphere from Pt crucibles by means of “Kristall 3M” setup with inductive heating and an automated control diameter system of growing crystal along the crystallographic axis [001]. The pulling changed within 1–3 mm/h and the rotational speed was varied in the range of 15–20 rpm. Grown $\text{PbWO}_4 + \text{PbMoO}_4$ crystals were used as a charge for growth of solid solution single crystals. It was done for better purification of solid solution single crystals. Y and Nb were added into initial mixture to prevent formation of color centers. The procedure and parameters of solid solution crystal growth were the same as for $\text{PbWO}_4 + \text{PbMoO}_4$ crystals. To minimize thermo-elastic stresses, the solid solution single crystals were annealed in air after the growth. The grown solid solution single crystals were transparent and free of color centers, impurity phases, crystal cracking and gas bubble inclusions. Typical dimensions of grown solid solution crystals were up to 30 mm in diameter and up to 70 mm in length. Dimensions of the investigated samples were $10 \times 10 \times 15 \text{ mm}^3$. All tested samples were anti-reflection coated in the spectral range from 1000 to 1400 nm.

Figure 1 demonstrates polarized spontaneous Raman spectra of $\text{Pb}(\text{MoO}_4)_{1-x}(\text{WO}_4)_x$ with $x = 0, 0.5, 0.8,$ and 1.0 for parallel ($\mathbf{E} \parallel \mathbf{c}$) and perpendicular ($\mathbf{E} \perp \mathbf{c}$) vector polarization relative to the optical crystal axis. The spectra are normalized to the most intense Raman line of each crystal (at $\mathbf{E} \perp \mathbf{c}$). The spectra were measured using a back-scattering scheme SPEX-Ramalog 1403 spectrometer (Horiba, Kyoto, Japan) excited by a 510.6-nm copper vapor laser with the spectral resolution of 0.5 cm^{-1} and scanning step of 0.2 cm^{-1} . It can be seen in Figure 1a,d that in the nominally pure ($x = 0$ and 1.0) PbMoO_4 and PbWO_4 crystals the difference of the bending ν_2 Raman mode frequencies is low ($\nu_2 = 318$ and 327 cm^{-1} , respectively) and comparable with their linewidth. In contrast to this, the stretching ν_1 Raman mode frequencies of PbMoO_4 and PbWO_4 are significantly distant ($\nu_1 = 870$ and 905 cm^{-1} , respectively). In both crystals, the high-frequency ν_1 Raman line is the most intense and it has approximately 1.33 times higher intensity at $\mathbf{E} \perp \mathbf{c}$ than at $\mathbf{E} \parallel \mathbf{c}$. On the contrary, the low-frequency ν_2 Raman line has higher intensity at $\mathbf{E} \parallel \mathbf{c}$ than at $\mathbf{E} \perp \mathbf{c}$ in both crystals. We should note that in PbWO_4 the ν_2 line has lower intensity relative to the ν_1 line in comparison with one in PbMoO_4 (especially at $\mathbf{E} \perp \mathbf{c}$). Figure 1b,c present the spectra of the mixed $\text{Pb}(\text{MoO}_4)_{1-x}(\text{WO}_4)_x$ crystal (for content of $x = 0.5$ and 0.8). The closely spaced bending ν_2 Raman modes of the molybdate and tungstate structures are coherently combined in one ν_2 vibrational line having one-mode behaviour [21] with the central frequency increasing from $\nu_2 = 321 \text{ cm}^{-1}$ up to $\nu_2 = 323 \text{ cm}^{-1}$ with increasing the tungstate content. Despite the fact that the stretching ν_1 Raman lines have here (Figure 1b,c) the two-mode behaviour [21], we found that in the mixed crystals the molybdate ($\nu_1 = 870 \text{ cm}^{-1}$) and tungstate ($\nu_1 = 905 \text{ cm}^{-1}$) stretching Raman modes interact with each other like the bending Raman modes.

Firstly, this is indicated by the widening of all the Raman modes. The ν_1 lines are widened from $\Delta\nu_1 = 6.0$ and 4.1 cm^{-1} in PbMoO_4 ($\nu_1 = 870 \text{ cm}^{-1}$) and PbWO_4 ($\nu_1 = 905 \text{ cm}^{-1}$), respectively, up to $\Delta\nu_1 = 7.2 \text{ cm}^{-1}$ for the 870 cm^{-1} line and $\Delta\nu_1 = 5.5 \text{ cm}^{-1}$ for the 905 cm^{-1} line in both mixed ($x = 0.5$ and 0.8) crystals. The ν_2 line is widened from $\Delta\nu_2 = 7.4$ and 7.7 cm^{-1} in PbMoO_4 ($\nu_2 = 318 \text{ cm}^{-1}$) and PbWO_4 ($\nu_2 = 327 \text{ cm}^{-1}$), respectively, up to $\Delta\nu_2 = 9.7 \text{ cm}^{-1}$ at $\mathbf{E} \parallel \mathbf{c}$ and $\Delta\nu_2 = 10.6 \text{ cm}^{-1}$ at $\mathbf{E} \perp \mathbf{c}$ for the combined ν_2 line in both mixed ($x = 0.5$ and 0.8) crystals. Secondly, this is indicated by the change of intensities of lines at $\mathbf{E} \parallel \mathbf{c}$ and $\mathbf{E} \perp \mathbf{c}$ when moving from one crystal to another.

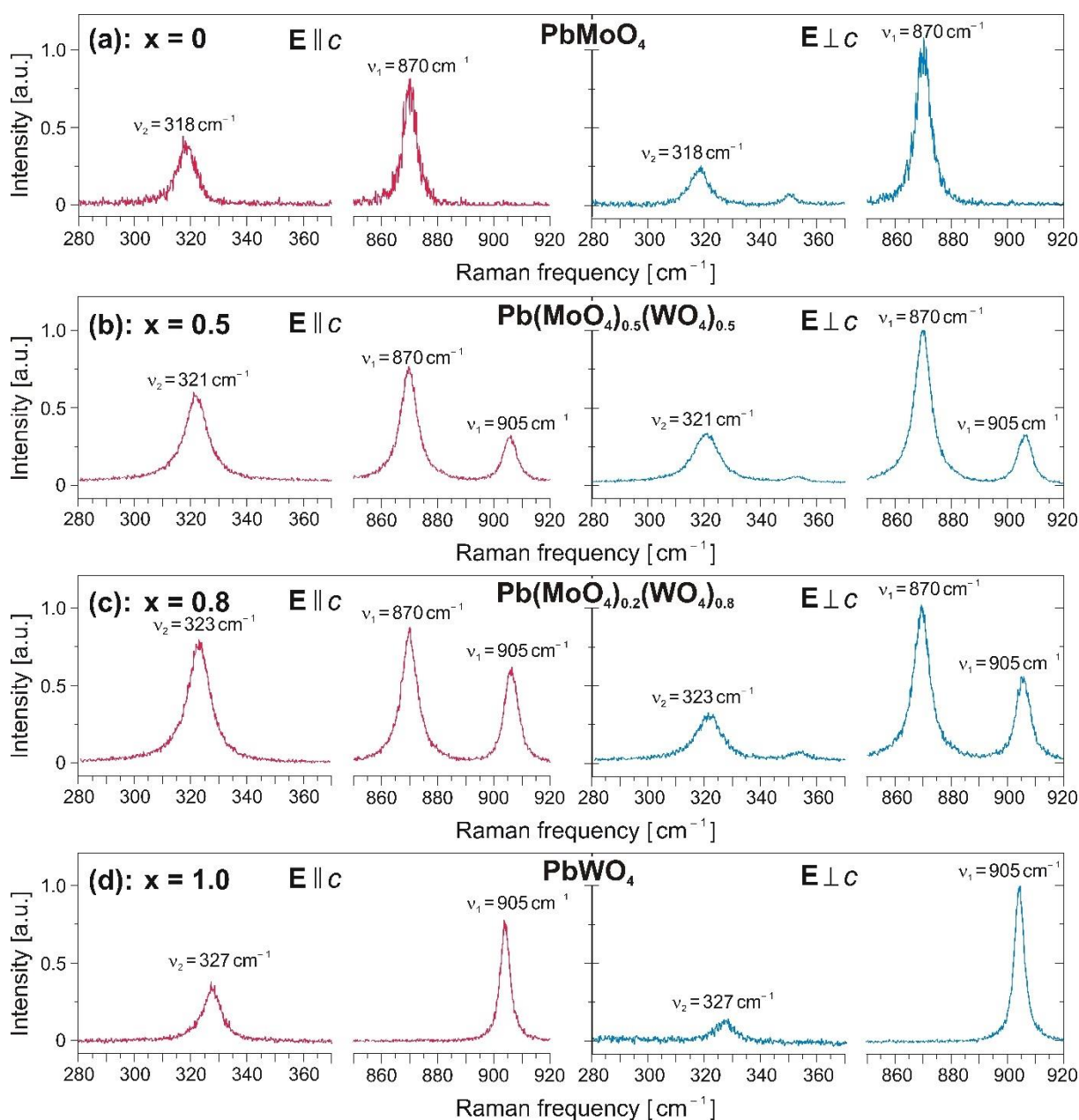


Figure 1. Polarized spontaneous Raman spectra of $\text{Pb}(\text{MoO}_4)_{1-x}(\text{WO}_4)_x$ at (a) $x = 0$, (b) $x = 0.5$, (c) $x = 0.8$, (d) $x = 1.0$ for parallel ($E \parallel c$) and perpendicular ($E \perp c$) orientation of the radiation polarization vector relative to the crystal optical axis.

Figure 1b shows that in the mixed $\text{Pb}(\text{MoO}_4)_{0.5}(\text{WO}_4)_{0.5}$ crystal with the equal molybdate and tungstate content, the molybdate ν_1 line has higher intensity and therefore stronger $(\text{MoO}_4)^{2-}$ vibration influences weaker $(\text{WO}_4)^{2-}$ vibration. This results in an increase in the 905 cm^{-1} line intensity at $E \parallel c$ up to that at $E \perp c$ in contrast to those in the nominally pure PbWO_4 crystal (Figure 1d) where it is 1.33 times lower at $E \parallel c$ than at $E \perp c$. The combined ν_2 line intensity in $\text{Pb}(\text{MoO}_4)_{0.5}(\text{WO}_4)_{0.5}$ (Figure 1b) also increases more at $E \parallel c$ than at $E \perp c$ in comparison with PbMoO_4 (Figure 1a). We believe that the interaction of vibrations of the $(\text{MoO}_4)^{2-}$ and $(\text{WO}_4)^{2-}$ anionic groups occurs through the Pb^{2+} cation having a high degree of covalent bond with oxygen. This covalent bond is directed mainly along the crystal optical axis, therefore the $E \parallel c$ orientation is suitable for more intensive Raman scattering in the mixed crystal. On other hand, the high-frequency Raman line has higher intensity at $E \perp c$ in the nominally pure PbMoO_4 and PbWO_4 crystals.

Taking into account the stronger $(\text{MoO}_4)^{2-}$ vibration, the tungstate content ratio was increased up to $x = 0.8$ to equalize the contributions of the molybdate and tungstate components to Raman scattering in the mixed $\text{Pb}(\text{MoO}_4)_{0.2}(\text{WO}_4)_{0.8}$ crystal. Figure 1c shows that in this crystal, intensities of the $\nu_1 = 905 \text{ cm}^{-1}$ and $\nu_2 = 323 \text{ cm}^{-1}$ Raman lines have increased only slightly at $\text{E} \perp c$, but they have increased much more at $\text{E} \parallel c$ and became comparable with the molybdate $\nu_1 = 870 \text{ cm}^{-1}$ Raman line intensity. Also note that even the molybdate $\nu_1 = 870 \text{ cm}^{-1}$ line intensity has slightly increased at $\text{E} \parallel c$ in comparison with the previous case (Figure 1b, $x = 0.5$). It can be explained by coherent interaction of the equalized $(\text{MoO}_4)^{2-}$ and $(\text{WO}_4)^{2-}$ vibrations through the covalent bond of the Pb^{2+} cation with oxygen directed mainly along the crystal optical axis.

3. Experimental Setup

Figure 2 shows the experimental setup. It is similar to that used in the previous works [17–19] using other Raman-active crystals. The Raman laser with an external ring cavity based on each Raman-active crystal under study was synchronously pumped by repetitively pumped, 36-ps, 150-MHz, 330-nJ Nd:GdVO₄ laser at a wavelength of $\lambda_0 = 1063 \text{ nm}$ operating in quasi-continuous regime with the $500 \mu\text{s}$. The pumping was single-pass due to high transmission of both concave mirrors (PM and CM) of the Raman laser cavity. The half-wave plate allowed pumping of the Raman-active crystal at either $\text{E} \parallel c$ or $\text{E} \perp c$. The lens FL focused the pump beam into an approximately $30 \times 35 \mu\text{m}^2$ spot in the Raman-active crystal in order to achieve the best possible mode matching with the Raman laser cavity mode. We used two output couplers (OC1 and OC2, both flat mirrors) with reflectivity distributions shown in Table 1 for efficient single first-order SRS (using OC1) and for multi-wavelength multi-order combined shift SRS (using OC2). The condition of synchronous pumping was adjusted by flat mirror FM on the precise translation stage.

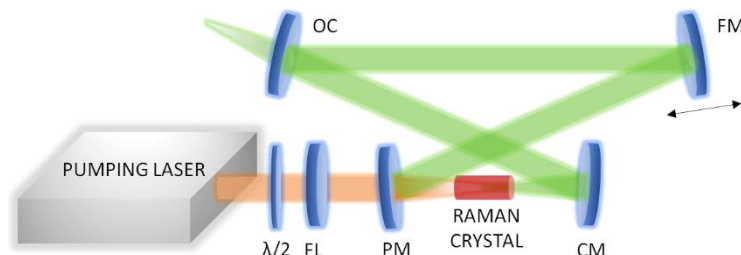


Figure 2. Experimental setup of synchronously pumped Raman laser.

Table 1. Reflectivities of two output couplers at the oscillated SRS wavelengths.

	OC1	OC
R [%] @ 1128/1132 nm ($\nu_1 - \nu_2$ shifted SRS component)	98.4/98.0	99.7/99.7
R [%] @ 1171/1176 nm (ν_1 shifted Stokes SRS component)	87.0/88.0	99.5/99.4
R [%] @ 1217/1222 nm ($\nu_1 + \nu_2$ shifted SRS component)	86.5/84.0	89.8/83.5
R [%] @ 1250 nm ($\nu_1 + \nu_1 - \nu_2$ shifted SRS component)	39.8	33.8
R [%] @ 1266/1272 nm ($\nu_1 + \nu_2 + \nu_2$ shifted SRS component)	44.2/53.5	50.7/53.4
R [%] @ 1303/1316 nm ($\nu_1 + \nu_1$ shifted SRS component)	69.6/66.4	17.5/28.5
R [%] @ 1360 nm ($\nu_1 + \nu_1 + \nu_2$ shifted SRS component)	11.0	16.7
R [%] @ 1128/1132 nm ($\nu_1 - \nu_2$ shifted SRS component)	98.4/98.0	99.7/99.7

The individual generated SRS components were separated by a set of calibrated long-pass filters (Thorlabs, Newton, NJ, USA). The output average power was measured by a power meter (Standa 11PMK 15SH5, Vilnius, Lithuania) and output pulse energy was calculated from the knowledge of repetition rate and duty cycle, respectively. For measuring of pulse duration, a laboratory designed non-collinear second harmonics generation autocorrelator based on a LiIO_3 crystal with temporal resolution of 23 fs was used. The mea-

sured autocorrelation curves were fitted by Gaussian function and duration was calculated at FWHM.

4. SRS in PbMoO_4 and PbWO_4

As in our previous works [17–19], SRS oscillation was achieved after precise synchronization of the Raman laser cavity length with the repetition rate of the pump laser. The synchronization must be tuned for each pumping orientation ($E \parallel c$ and $E \perp c$) because of high birefringence of the investigated crystals [19]. Figure 3 shows the obtained output radiation spectra and the output beam profiles in the synchronously pumped Raman lasers based on the nominally pure PbMoO_4 and PbWO_4 crystals for the case of the highest pump pulse energy of 330 nJ.

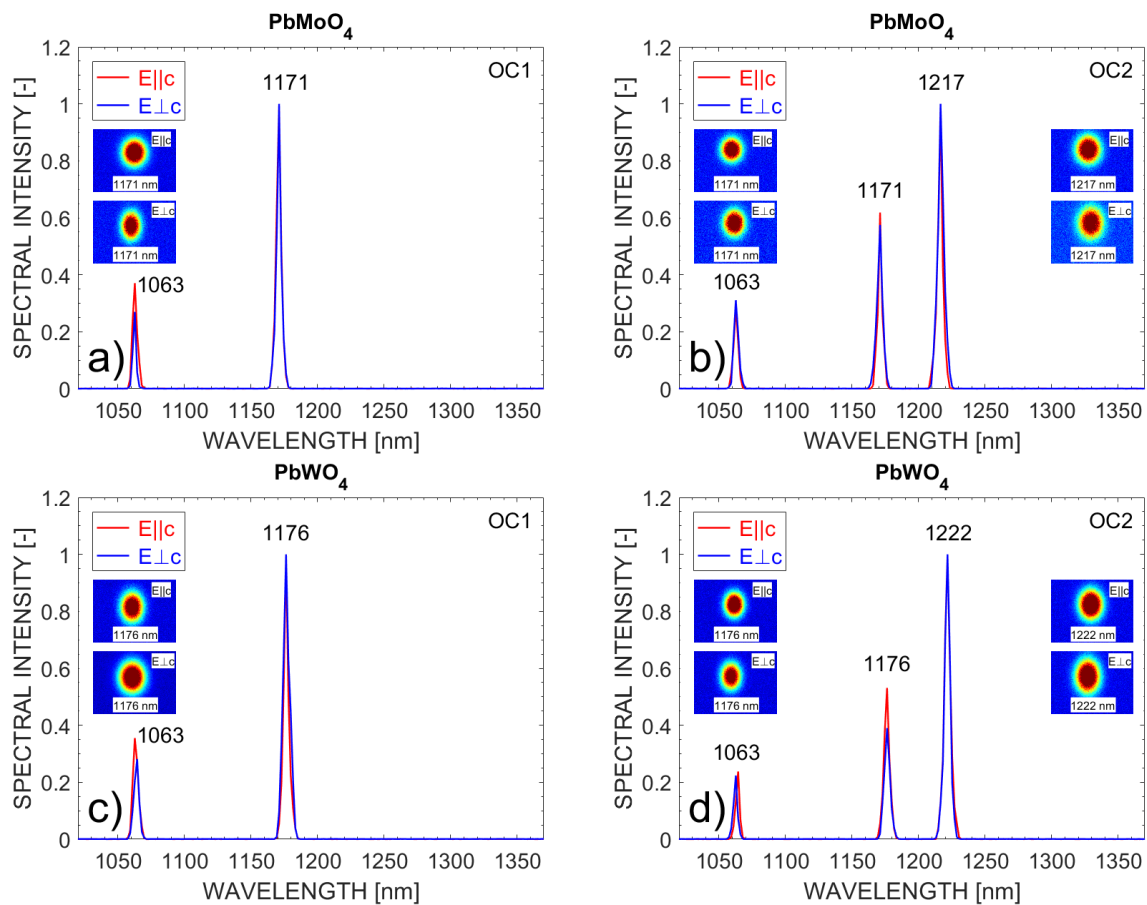


Figure 3. Output radiation spectra of the synchronously pumped PbMoO_4 with OC1 (a) and OC2 (b), PbWO_4 Raman lasers with OC1 (c) and OC2 (d).

We can see that using the OC1 output coupler resulted in generation of only one Stokes component at the wavelength of 1171 or 1176 nm with the high-frequency Raman shift of $\nu_1 = 870$ or 905 cm^{-1} for PbMoO_4 or PbWO_4 , respectively. In the case of the setup with the OC2, the additional Stokes component at the wavelength of 1217 or 1222 nm with the combined frequency shift of $\nu_1 + \nu_2 = 870 + 318$ or $905 + 327 \text{ cm}^{-1}$ was oscillated for PbMoO_4 or PbWO_4 , respectively. The beam profiles measured by a CCD camera were close to the fundamental transversal mode and showed astigmatism due to the nonzero-angle of incidence on concave mirrors used inside the Raman laser cavity. The beam profile dimensions for the $(\nu_1 + \nu_2)$ -shifted SRS components were larger due to the beam diffraction divergence increase with the wavelength.

The dependencies of the output SRS pulse energy on the input pulse energy in the synchronously pumped PbMoO_4 and PbWO_4 Raman lasers with the OC1 and OC2 output

couplers in the case of perfect synchronous pumping (taken as zero detuning of the cavity length) are presented in Figure 4. It can be seen from Figure 4a,c that using the OC1 output coupler led to efficient generation of the single ν_1 -shifted Stokes component with linear growth of energy output. In general, the SRS generation with higher slope efficiency and lower threshold was achieved for $E \perp c$. The increase in the oscillation threshold for $E \parallel c$ is caused by the decrease in the Raman gain because the losses were almost constant. It can be assumed that a ratio of the oscillation thresholds at $E \perp c/E \parallel c$ (103 nJ/128 nJ for PbMoO_4 and 121 nJ/139 nJ for PbWO_4) is close to a ratio of intensities of the ν_1 Raman modes at $E \parallel c/E \perp c$ for each crystal (see Figure 1a,d). It is also necessary to pay attention to the observed effect of increasing slope efficiency of oscillation from 25.7% to 44.7% for PbMoO_4 and from 20.0% to 33.8% for PbWO_4 with the change of the pumping orientation from $E \parallel c$ to $E \perp c$ that is accompanied by increase in the Raman gain with no change of losses. Earlier, similar effect was observed in many synchronously pumped Raman lasers based on GdVO_4 [28], SrWO_4 [18,29], and PbMoO_4 [19] active crystals via a change of the single-pass Raman gain by a change of the crystal length or pumping orientation. A possible explanation of the effect may be the action of synchronous pumping as it was proposed in work [19].

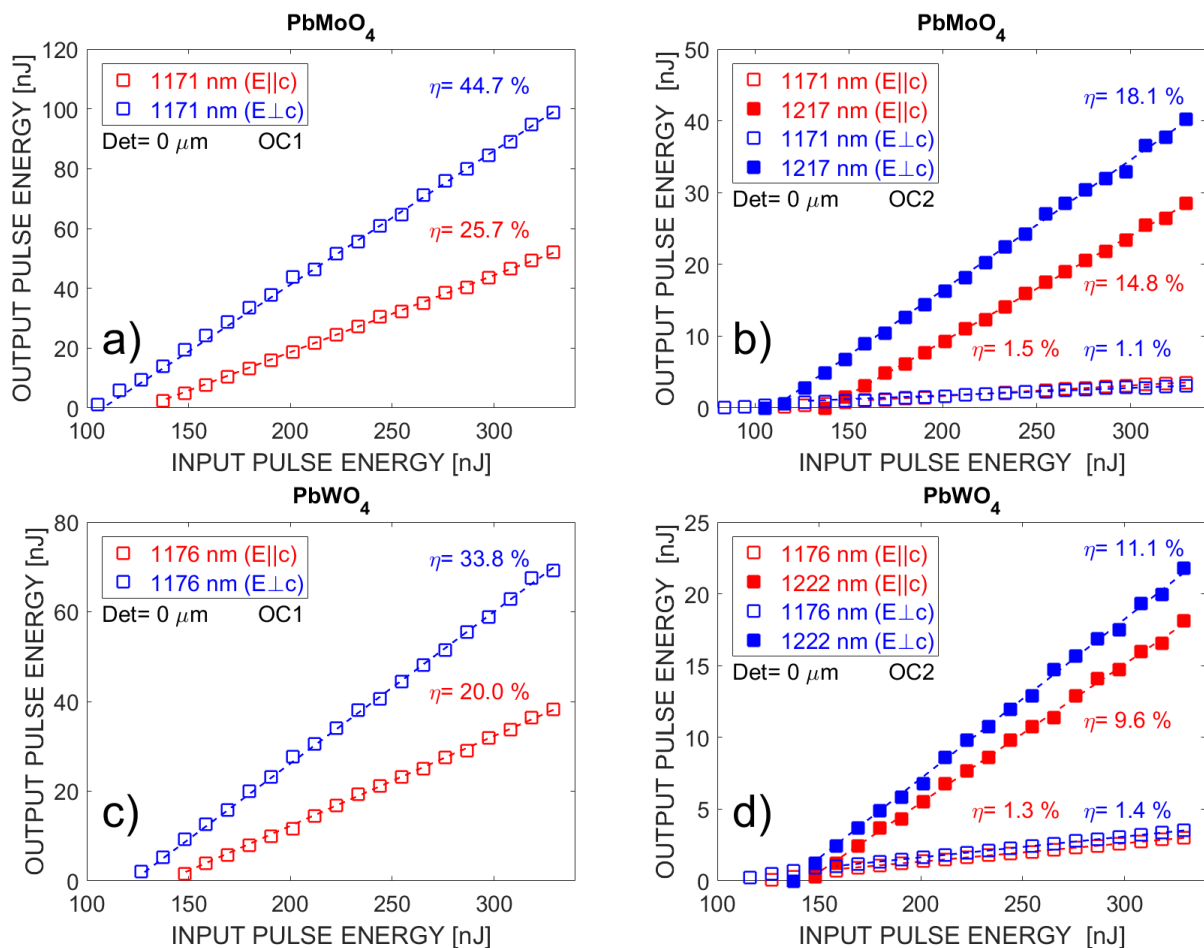


Figure 4. The output SRS pulse energy versus the input pump pulse energy in the synchronously pumped Raman laser based on (a) PbMoO_4 with OC1, (b) PbMoO_4 with OC2, (c) PbWO_4 with OC1, and (d) PbWO_4 with OC2.

It can be seen in Figure 4b,d that in the case of PbMoO_4 (PbWO_4) using the OC2 output coupler resulted in more efficient oscillation of the 1217 (1222) nm second Stokes component with the $\nu_1 + \nu_2$ combined frequency shift. The lower efficiency of the 1171

(1176) nm ν_1 -shifted first Stokes component was caused by high reflection of OC2 at the 1171 (1176) nm wavelength (see Table 1).

The SRS generation at 1217 (1222) nm with lower threshold was achieved under $E \perp c$ pumping (111 nJ at $E \perp c$ against 137 nJ at $E \parallel c$ for $PbMoO_4$ and 136 nJ at $E \perp c$ against 142 nJ at $E \parallel c$ for $PbWO_4$). Moreover, the slope efficiencies were higher (18.1% at $E \perp c$ against 14.8% at $E \parallel c$ for $PbMoO_4$ and 11.1% at $E \perp c$ against 9.6% at $E \parallel c$ for $PbWO_4$). These output parameters were measured despite the ν_2 line is more intensive in the polarized spontaneous Raman spectra at $E \parallel c$ than at $E \perp c$ for both $PbMoO_4$ and $PbWO_4$ (see Figure 1a,d). Earlier in [19], similar effect was observed for the two times longer $PbMoO_4$ active element. This phenomenon can be explained by more intense intracavity pumping of the second cascade SRS by the ν_1 -shifted first Stokes component that oscillated more efficiently at $E \perp c$.

Figure 5 demonstrates the output radiation characteristics of the $PbMoO_4$ and $PbWO_4$ Raman lasers with the OC2 output coupler as a function of the cavity length detuning at the optimum $E \perp c$ orientation for the highest pump pulse energy of 330 nJ. The dependencies are similar to those of many active media in the synchronously pumped Raman laser with the combined frequency shift tested before [17–19,28,29]. The case of cavity length detuning with the lowest SRS threshold is marked as zero detuning. In particular, the ($\nu_1 + \nu_2$)-shifted Stokes pulses had shortened duration amounting 7 ps at zero detuning and even shorter at positive detuning of the cavity length. The shortest pulse duration was measured to be 1.33 (1.41) ps and 1.22 (1.27) ps at $E \perp c$ ($E \parallel c$) for $PbMoO_4$ and $PbWO_4$, respectively, at +50 μm cavity length detuning. The values are comparable with an inverse half-width of the ν_2 Raman line amounting $1/(\pi \cdot c \cdot \Delta\nu_2) = 1.43$ ps and 1.38 ps for $PbMoO_4$ and $PbWO_4$, respectively.

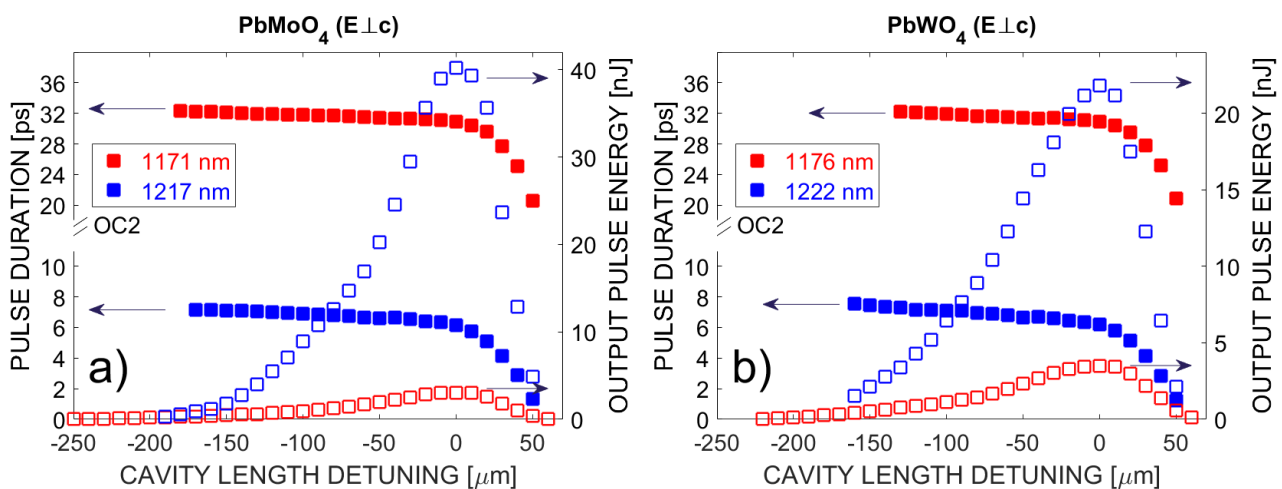


Figure 5. Output pulse energy and pulse duration versus the Raman laser cavity length detuning with OC2 for the synchronously pumped (a) $PbMoO_4$ and (b) $PbWO_4$ Raman lasers at the optimum $E \perp c$ orientation.

5. SRS in $Pb(MoO_4)_{0.5}(WO_4)_{0.5}$ and $Pb(MoO_4)_{0.2}(WO_4)_{0.8}$

Figure 6 demonstrates the obtained output radiation spectra and the output beam profiles in the synchronously pumped Raman lasers based on the mixed $Pb(MoO_4)_{0.5}(WO_4)_{0.5}$ and $Pb(MoO_4)_{0.2}(WO_4)_{0.8}$ crystals. The beam profiles are close to the fundamental transversal mode as for the nominally pure crystals.

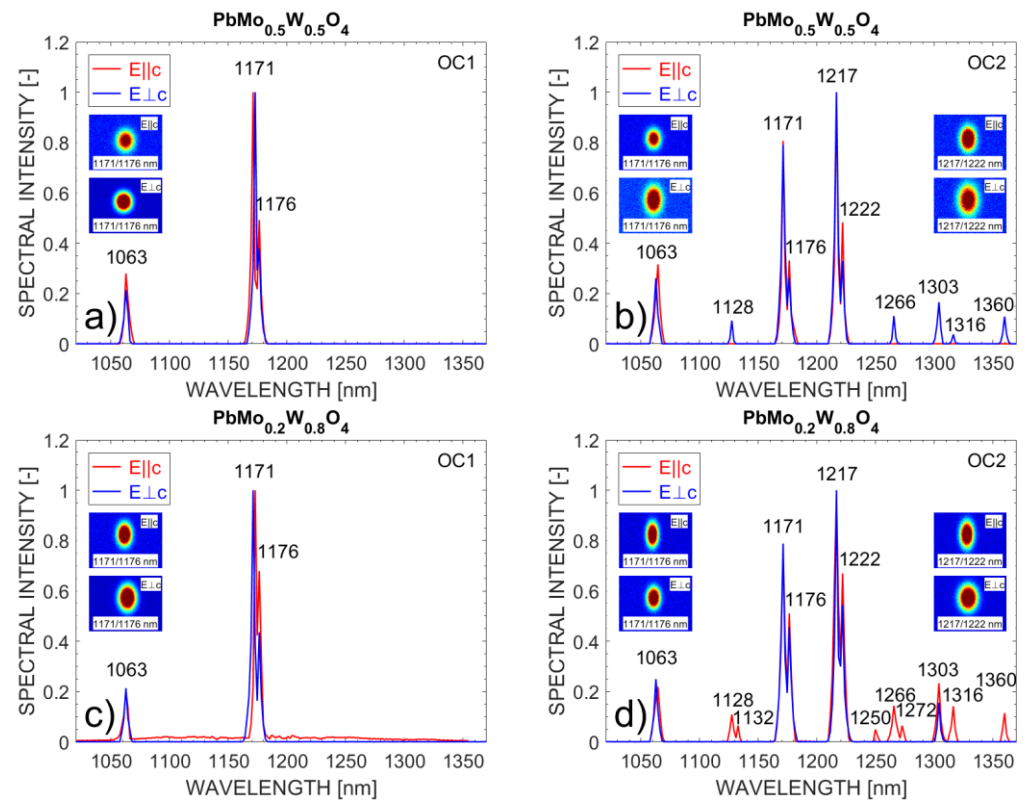


Figure 6. Output radiation spectra of the synchronously pumped Raman lasers based on (a) $\text{Pb}(\text{MoO}_4)_{0.5}(\text{WO}_4)_{0.5}$ with OC1, (b) $\text{Pb}(\text{MoO}_4)_{0.5}(\text{WO}_4)_{0.5}$ with OC2, (c) $\text{Pb}(\text{MoO}_4)_{0.2}(\text{WO}_4)_{0.8}$ with OC1, and (d) $\text{Pb}(\text{MoO}_4)_{0.2}(\text{WO}_4)_{0.8}$ with OC2.

It can be seen from Figure 6a,c that using the OC1 resulted again in oscillation of only ν_1 -shifted first Stokes component but with the wavelength doublet of 1171/1176 nm corresponding to both the high-frequency stretching Raman modes of $\nu_1 = 870$ and 905 cm^{-1} of the molybdate and tungstate contents, respectively. Note that the tungstate SRS component at 1176 nm has lower intensity than the molybdate SRS component at 1171 nm in the doublet, but using $\text{Pb}(\text{MoO}_4)_{0.2}(\text{WO}_4)_{0.8}$ made this situation better for the tungstate SRS component.

Figure 6b,d show the spectra observed with the OC2. The second Stokes component at the wavelength doublet of 1217/1222 nm with the bending mode ν_2 frequency shift from the ν_1 -shifted first Stokes doublet also oscillated in both mixed crystals. Using the optimum pumping orientation allowed to additionally obtain the $(\nu_1 + \nu_1)$ - and $(\nu_1 - \nu_2)$ -shifted second-order SRS components and even the third-order Stokes components with the combined frequency shifts of $\nu_1 + \nu_2 + \nu_2$ and $\nu_1 + \nu_1 + \nu_2$. The optimum pumping orientation was different for these mixed crystals. For $\text{Pb}(\text{MoO}_4)_{0.5}(\text{WO}_4)_{0.5}$ it was $\mathbf{E} \perp c$, i.e., the same as for the nominally pure PbMoO_4 and PbWO_4 crystals. However, for $\text{Pb}(\text{MoO}_4)_{0.2}(\text{WO}_4)_{0.8}$ the $\mathbf{E} \parallel c$ orientation turned out to be better for multi-wavelength operation. Also, three cascades of SRS in the 14-mm long mixed crystals are different from two cascades of SRS in the 25-mm long nominally pure crystals. This can be explained by the fact that parametric Raman coupling provides more efficient multi-cascade SRS in shorter crystals than in longer crystals [18]. This is confirmed by the presence of the ν_2 -shifted anti-Stokes components in the second $(\nu_1 - \nu_2)$ and third $(\nu_1 + \nu_1 - \nu_2)$ cascades of SRS in the mixed crystals. Also note that in $\text{Pb}(\text{MoO}_4)_{0.2}(\text{WO}_4)_{0.8}$ a larger part of the third-cascade SRS wavelengths are doublets in contrast to $\text{Pb}(\text{MoO}_4)_{0.5}(\text{WO}_4)_{0.5}$ where are mostly singlets corresponding to the dominant molybdate content (see the wavelengths identification in Figure 6 and Table 1).

Figure 7 shows output pulse energy of ν_1 -shifted 1171/1176 nm and $(\nu_1 + \nu_2)$ -shifted 1217/1222 nm SRS components in the mixed crystals as a function of the input pulse energy. These are the same SRS components as in the nominally pure crystals in Figure 4. The oscillation character in the case of $\text{Pb}(\text{MoO}_4)_{0.5}(\text{WO}_4)_{0.5}$ with the OC1 was similar to the nominally pure crystals (Figure 4a,c): at $\mathbf{E} \perp c$ the first Stokes oscillation threshold was lower (130 nJ against 168 nJ) and slope efficiency was higher (18.6% against 14.7%) than at $\mathbf{E} \parallel c$. However, again, for $\text{Pb}(\text{MoO}_4)_{0.2}(\text{WO}_4)_{0.8}$, the situation using the OC1 was different (Figure 7c): at $\mathbf{E} \perp c$ the first Stokes oscillation threshold was higher (157 nJ against 145 nJ) and slope efficiency was lower (17.5% against 21.1%) than at $\mathbf{E} \parallel c$. We can also see that slope efficiencies for the $\text{Pb}(\text{MoO}_4)_{0.5}(\text{WO}_4)_{0.5}$ and $\text{Pb}(\text{MoO}_4)_{0.2}(\text{WO}_4)_{0.8}$ crystals were lower than for the PbMoO_4 and PbWO_4 crystals. These characteristics can be explained by shorter length of the mixed crystals (14 mm against 25 mm) from the point of view of the above-mentioned effect of higher slope efficiency at higher single-pass Raman gain.

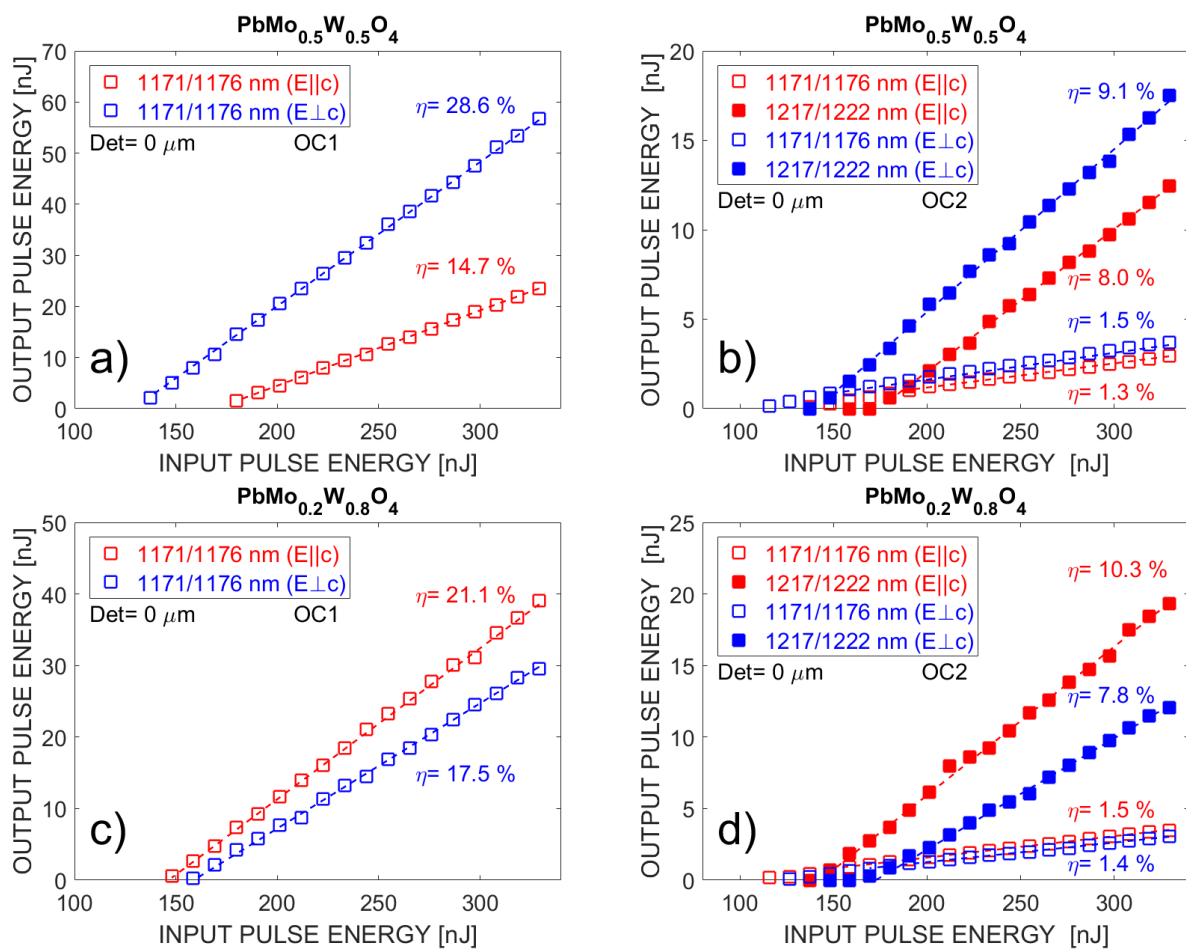


Figure 7. The output SRS pulse energy versus the input pump pulse energy in the synchronously pumped Raman laser based on (a) $\text{Pb}(\text{MoO}_4)_{0.5}(\text{WO}_4)_{0.5}$ with OC1, (b) $\text{Pb}(\text{MoO}_4)_{0.5}(\text{WO}_4)_{0.5}$ with OC2, (c) $\text{Pb}(\text{MoO}_4)_{0.2}(\text{WO}_4)_{0.8}$ with OC1, and (d) $\text{Pb}(\text{MoO}_4)_{0.2}(\text{WO}_4)_{0.8}$ with OC2.

Recently, the comparative measurement procedure using the oscillation threshold data in the same conditions was developed to define the Raman gain for PbMoO_4 at 1063 nm, which was measured to be $g = 5.0 \text{ cm/GW}$ at $\mathbf{E} \perp c$ [19]. Now we used this procedure for the measurement of the Raman gain for all the crystals under study at both pumping polarizations in comparison with the value measured before for PbMoO_4 . The results of the comparative measurement are shown in Table 2 (see [19] for details). For PbMoO_4 and PbWO_4 , the refractive index data were taken from [19,30]; for both the mixed crystals they were taken as the average values for PbMoO_4 and PbWO_4 .

Table 2. Measurement results of Raman gain for the crystals under study at the $\mathbf{E} \perp c$ ($\mathbf{E} \parallel c$) pumping orientation, where L is the crystal length, L_{eff} is the effective length of Raman interaction considering at beam focusing [19], E_{th} is the threshold pump pulse energy, g is the Raman gain calculated as in [19].

Crystal	PbMoO ₄	PbWO ₄	Pb(MoO ₄) _{0.5} (WO ₄) _{0.5}	Pb(MoO ₄) _{0.2} (WO ₄) _{0.8}
L [cm]	2.5	2.5	1.4	1.4
L_{eff} [cm]	1.39 (1.35)	1.34 (1.32)	1.04 (1.03)	1.04 (1.03)
E_{th} [nJ]	103 (128)	121 (139)	130 (168)	157 (145)
$E_{th} \cdot L_{eff}$ [nJ·cm]	143 (173)	162 (184)	135 (173)	163 (149)
g [cm/GW]	5.0 (4.1)	4.4 (3.9)	5.3 (4.1)	4.4 (4.8)

We can see that for Pb(MoO₄)_{0.5}(WO₄)_{0.5} the Raman gain at both the pumping orientations is close to that for PbMoO₄ (the difference is not higher than the measurement error). On the contrary, for Pb(MoO₄)_{0.2}(WO₄)_{0.8} at $\mathbf{E} \perp c$, the Raman gain is close to that for PbWO₄ at $\mathbf{E} \perp c$. But for Pb(MoO₄)_{0.2}(WO₄)_{0.8} at $\mathbf{E} \parallel c$, the Raman gain is anomalously high in comparison with all other crystals at $\mathbf{E} \parallel c$ and especially for Pb(MoO₄)_{0.2}(WO₄)_{0.8} at $\mathbf{E} \perp c$. It can be explained by the most efficient coherent interaction of equalized vibrations of the molybdate and tungstate anionic groups due to their optimum relative content. As one can see from Figure 7b, using the OC2 for Pb(MoO₄)_{0.5}(WO₄)_{0.5} the oscillation was similar as for PbMoO₄ and PbWO₄ (Figure 4b,d), in particular, the $\mathbf{E} \perp c$ pumping orientation was better for the ($\nu_1 + \nu_2$)-shifted output too. We achieved ($\nu_1 + \nu_2$)-shifted Stokes component at 1217/1222 nm with slope efficiency of 9.1% and 8.0% at oscillation threshold of $E_{th} = 140$ and 171 nJ for $\mathbf{E} \perp c$ and $\mathbf{E} \parallel c$, respectively. Nevertheless, oscillation of the ν_1 -shifted 1171/1176 nm SRS component has lower efficiency (<1.5%), with a lower oscillation threshold of $E_{th} = 107$ and 133 nJ for $\mathbf{E} \perp c$ and $\mathbf{E} \parallel c$, respectively, due to the high-Q cavity at 1171/1176 nm. It is necessary to note that for the 1217/1222 nm output, the product $E_{th} \cdot L_{eff} = 146$ (176) nJ·cm at $\mathbf{E} \perp c$ ($\mathbf{E} \parallel c$) was comparable with $E_{th} \cdot L_{eff} = 154$ (185) nJ·cm at $\mathbf{E} \perp c$ ($\mathbf{E} \parallel c$) for PbMoO₄. On the other hand, it is distinctly lower than $E_{th} \cdot L_{eff} = 182$ (187) nJ·cm at $\mathbf{E} \perp c$ ($\mathbf{E} \parallel c$) for PbWO₄ (L_{eff} was taken from Table 2). Therefore, it can be said that SRS in the mixed Pb(MoO₄)_{0.5}(WO₄)_{0.5} crystal using OC2 as well as using OC1 (see $E_{th} \cdot L_{eff}$ in Table 2) was mostly initiated by the stronger (MoO₄)²⁻ vibrations. Participation of the (WO₄)²⁻ vibrations was more appreciable at $\mathbf{E} \parallel c$ as can be seen from the SRS spectra (Figure 6a,b). This can be explained by better coupling between the (MoO₄)²⁻ and (WO₄)²⁻ vibrations through the partly covalent bond with the Pb²⁺ cation directed along the crystal optical axis.

The most interesting results can be seen for Pb(MoO₄)_{0.2}(WO₄)_{0.8} from Figure 7d. At $\mathbf{E} \perp c$ for the 1217/1222 nm output it had predictably higher oscillation threshold of 167 nJ and lower slope efficiency of 7.8% than for Pb(MoO₄)_{0.5}(WO₄)_{0.5} (140 nJ and 9.1%) because of the lower molybdenum content. Another situation was seen at $\mathbf{E} \parallel c$ for the 1217/1222 nm output where we can see the highest slope efficiency of 10.3% for Pb(MoO₄)_{0.2}(WO₄)_{0.8} among both the mixed crystals with low oscillation threshold of 141 nJ close to the lowest value for Pb(MoO₄)_{0.5}(WO₄)_{0.5} (140 nJ at $\mathbf{E} \perp c$). Similarly, as in the previous cases, it can be explained by the optimum relative Mo/W content (20/80%) with the best coupling between the (MoO₄)²⁻ and (WO₄)²⁻ vibrations at $\mathbf{E} \parallel c$. This time it is not only for the ν_1 mode but also for the ν_2 mode. As a result, in Pb(MoO₄)_{0.2}(WO₄)_{0.8} with the OC2 and $\mathbf{E} \parallel c$, the 1171/1176 nm first-order Stokes radiation efficiently converted on the intense ν_1 vibration doublet which was efficiently converted into the 1217/1222 nm second-order Stokes component on the coherently combined intense ν_2 Raman mode. The summary of experimental results can be seen in Table 3.

Table 3. Output characteristics of synchronously pumped Raman laser under $E \perp c$ ($E \parallel c$) pumping for setup with OC1 and OC2. E_{th} means is the threshold pump pulse energy and η is the slope efficiency for ν_1 - and $(\nu_1 + \nu_2)$ - shifted components.

Crystal	PbMoO ₄	PbWO ₄	Pb(MoO ₄) _{0.5} (WO ₄) _{0.5}	Pb(MoO ₄) _{0.2} (WO ₄) _{0.8}
Setup with OC1				
$E_{th}(\nu_1)$ [nJ]	103 (128)	121 (139)	130 (168)	157 (145)
$\eta(\nu_1)$ [%]	44.7 (25.7)	33.8 (20.0)	28.6 (14.7)	17.5 (21.1)
Setup with OC2				
$E_{th}(\nu_1)$ [nJ]	82 (107)	105 (112)	107 (133)	123 (116)
$\eta(\nu_1)$ [%]	1.5 (1.1)	1.4 (1.3)	1.5 (1.3)	1.4 (1.5)
$E_{th}(\nu_1 + \nu_2)$ [nJ]	111 (137)	136 (142)	140 (171)	167 (141)
$\eta(\nu_1 + \nu_2)$ [%]	18.1 (14.8)	11.1 (9.6)	9.1 (8.0)	7.8 (10.3)

Figure 8 shows the cavity length detuning curves for the mixed crystals with the optimum pumping orientations [Pb(MoO₄)_{0.5}(WO₄)_{0.5} at $E \perp c$ and Pb(MoO₄)_{0.2}(WO₄)_{0.8} at $E \parallel c$] at pump pulse energy of 330 nJ and with the OC2. Again, the $(\nu_1 + \nu_2)$ -shifted Stokes pulses had shortened pulse duration of 7 ps at zero detuning and shorter at positive detuning of cavity length, but for both mixed crystals we have achieved the shortest pulse durations at +50 μm cavity length detuning in comparison with not only PbMoO₄ and PbWO₄ but also with all the investigated nominally pure scheelite-like tungstate and molybdate crystals: 1.19 (1.44) ps at $E \perp c$ ($E \parallel c$) for Pb(MoO₄)_{0.5}(WO₄)_{0.5} and 1.21 (1.16) ps at $E \perp c$ ($E \parallel c$) for Pb(MoO₄)_{0.2}(WO₄)_{0.8}, respectively. These values at the optimum pumping orientations are close to the inverse half-width of the widened combined ν_2 Raman line amounting $1/(\pi \cdot c \cdot \Delta\nu_2) = 1.0$ (1.1) ps at $E \perp c$ ($E \parallel c$). The generation of shorter pulses at 1217/1222 nm in the mixed structure with the higher tungstate content confirms the coupling of the pulse duration with the width of the ν_2 line, since it is wider in PbWO₄ ($\Delta\nu_2 = 7.7 \text{ cm}^{-1}$) than in PbMoO₄ ($\Delta\nu_2 = 7.4 \text{ cm}^{-1}$).

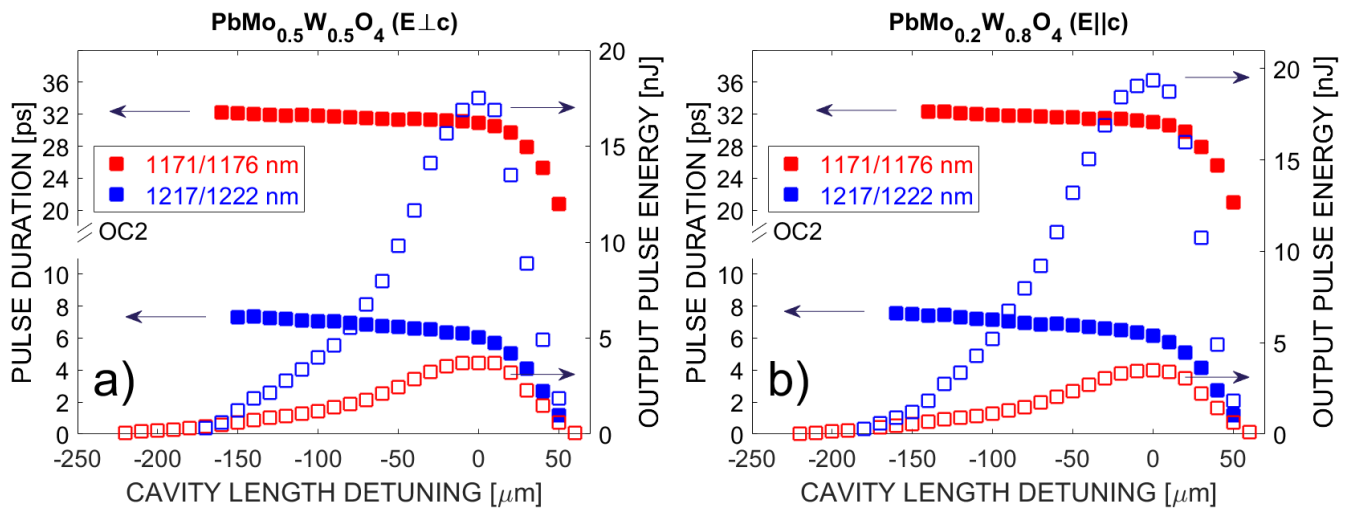


Figure 8. Output pulse energy and pulse duration versus the Raman laser cavity length detuning with OC2 for the synchronously pumped Raman lasers based on (a) Pb(MoO₄)_{0.5}(WO₄)_{0.5} at the optimum $E \perp c$ orientation and (b) Pb(MoO₄)_{0.2}(WO₄)_{0.8} at the optimum $E \parallel c$ orientation.

6. Conclusions

We have presented a comparison of the characteristics of spontaneous and stimulated Raman scattering in Pb(MoO₄)_{1-x}(WO₄)_x single crystals ($x = 0, 0.5, 0.8$, and 1.0) including both the high (ν_1) and low (ν_2) frequency internal anionic group vibrations. It was found that among these crystals, Pb(MoO₄)_{0.2}(WO₄)_{0.8} is the most promising for multi-wavelength

SRS on several Raman modes simultaneously. Thus is caused by the optimal relative Mo/W content corresponding to the most efficient coherent combination of the $(\text{MoO}_4)^{2-}$ and $(\text{WO}_4)^{2-}$ vibrations enhancing the output radiation characteristics of the synchronously pumped $\text{Pb}(\text{MoO}_4)_{0.2}(\text{WO}_4)_{0.8}$ Raman laser. We have achieved up to twelve oscillations of closely spaced SRS components in a range of 1128–1360 nm and the strongest pulse shortening down to 1.16 ps in comparison with not only PbMoO_4 and PbWO_4 , but also with all the nominally pure scheelite-like tungstate and molybdate crystals earlier investigated.

Author Contributions: Conceptualization, S.N.S.; methodology, M.F. and S.N.S.; software, M.F.; validation, P.G.Z. and V.K.; formal analysis, M.F., K.A.G. and S.N.S.; investigation, M.F., S.N.S., M.J., D.V. and V.E.S.; resources, M.B.K., A.N.S. and V.E.S.; data curation, M.B.K. and A.N.S.; writing—original draft preparation, M.F., S.N.S., M.J. and D.V.; writing—review and editing, M.F., S.N.S., M.J., D.V., P.G.Z. and V.K.; visualization, M.F.; supervision, P.G.Z. and V.K. All authors have read and agreed to the published version of the manuscript.

Funding: The presented Raman laser studies were funded by European Regional Development Fund—CZ.02.1.01/0.0/0.0/16_019/0000778. The Raman crystals characterization (Section 2) and solid solutions approximation (Section 5) were funded by Russian Science Foundation—Project No 22-22-00708 (<https://rscf.ru/project/22-22-00708/> [1 January 2019]).

Institutional Review Board Statement: Not applicable.

Informed Consent Statement: Not applicable.

Data Availability Statement: Not applicable.

Conflicts of Interest: The authors declare no conflict of interest.

References

1. Pinnow, D.A.; Van Uitert, L.G.; Warner, A.W.; Bonner, W.A. Lead molybdate: A melt-grown crystal with a high figure of merit for acousto-optic device applications. *Appl. Phys. Lett.* **1969**, *15*, 83–86. [[CrossRef](#)]
2. Coquin, G.A.; Pinnow, D.A.; Warner, A.W. Physical properties of lead molybdate relevant to acousto-optic device applications. *J. Appl. Phys.* **1971**, *42*, 2162–2168. [[CrossRef](#)]
3. Lecoq, P.; Dafinei, I.; Auffray, E.; Schneegans, M.; Korzhik, M.V.; Mishevitch, O.V.; Pavlenko, V.B.; Fedorov, A.A.; Annenkov, A.N.; Kostylev, V.L.; et al. Lead tungstate (PbWO_4) scintillators for LHC EM calorimetry. *Nucl. Instr. Meth. A* **1995**, *365*, 291–298. [[CrossRef](#)]
4. Danevich, F.A.; Grinyov, B.V.; Henry, S.; Kosmyna, M.B.; Kraus, H.; Krutyak, N.; Kudovbenko, V.M.; Mikhailik, V.B.; Nagornaya, L.L.; Nazarenko, B.P.; et al. Feasibility study of PbWO_4 and PbMoO_4 crystal scintillators for cryogenic rare events experiments. *Nucl. Instr. Meth. A* **2010**, *622*, 608–613. [[CrossRef](#)]
5. Kaminskii, A.A.; Eichler, H.J.; Ueda, K.; Klassen, N.V.; Redkin, B.S.; Li, L.E.; Findeisen, J.; Jaque, D.; Garcia-Sole, J.; Fernandez, J.; et al. Properties of Nd^{3+} -doped and undoped tetragonal PbWO_4 , $\text{NaY}(\text{WO}_4)_2$, CaWO_4 , and undoped monoclinic ZnWO_4 and CdWO_4 as laser-active and stimulated Raman scattering-active crystals. *Appl. Opt.* **1999**, *38*, 4533–4547. [[CrossRef](#)]
6. Kaminskii, A.A.; Bagayev, S.N.; Ueda, K.; Eichler, H.J.; Garcia-Sole, J.; Jaque, D.; Romero, J.J.; Fernandez, J.; Balda, R.; Butashin, A.V.; et al. Multiple Stokes and anti-Stokes picosecond generation, cw laser action at wavelengths of two stimulated-emission channels ${}^4\text{F}_{3/2} \rightarrow {}^4\text{I}_{11/2}$ and ${}^4\text{F}_{3/2} \rightarrow {}^4\text{I}_{13/2}$, and nanosecond self-SRS lasing in undoped and Nd^{3+} -doped tetragonal PbMoO_4 crystals. *Laser Phys.* **2001**, *11*, 1142–1146.
7. Gad, G.M.A.; Eichler, H.J.; Kaminskii, A.A. Highly efficient 1.3- μm second-Stokes PbWO_4 Raman laser. *Opt. Lett.* **2003**, *28*, 426–428. [[CrossRef](#)] [[PubMed](#)]
8. Basiev, T.T.; Zverev, P.G.; Karasik, A.Y.; Osiko, V.V.; Sobol, A.A.; Chunaev, D.S. Picosecond stimulated Raman scattering in crystals. *J. Exp. Theor. Phys.* **2004**, *99*, 934–941. [[CrossRef](#)]
9. Basiev, T.T.; Doroshenko, M.E.; Ivleva, L.I.; Osiko, V.V.; Kosmyna, M.B.; Komar, V.K.; Jelínková, H. Laser properties of selectively pumped Raman-active Nd^{3+} -doped molybdate and tungstate crystals. *Quantum Electron.* **2006**, *36*, 720–726. [[CrossRef](#)]
10. Ding, Z.; Ding, S.; Jia, H.; Liu, J.; Yang, L.; Huangfu, J.; Wang, S. Laser diode pumped, actively Q-switched, and mode-locked Nd:YAG/ PbWO_4 Raman laser. *Appl. Opt.* **2015**, *54*, 5375–5381. [[CrossRef](#)]
11. Basiev, T.T.; Sobol, A.A.; Voronko, Y.K.; Zverev, P.G. Spontaneous Raman spectroscopy of tungstate and molybdate crystals for Raman lasers. *Opt. Mater.* **2000**, *15*, 205–216. [[CrossRef](#)]
12. Zverev, P.G.; Basiev, T.T.; Sobol, A.A.; Ermakov, I.V.; Gellerman, W. BaWO_4 crystal for quasi-cw yellow Raman laser. *OSA TOPS* **2001**, *50*, 212–217.
13. Lin, J.; Pask, H.M. Cascaded self-Raman lasers based on 382 cm^{-1} shift in $\text{Nd}:\text{GdVO}_4$. *Opt. Express* **2012**, *20*, 15180–15185. [[CrossRef](#)] [[PubMed](#)]

14. Lin, H.Y.; Pan, X.; Huang, H.; Xiao, M.; Liu, X.; Sun, D.; Zhu, W.Z. Multi-wavelength passively Q-switched c-cut Nd:YVO₄ self-Raman laser with Cr⁴⁺:YAG saturable absorber. *Opt. Commun.* **2016**, *368*, 39–42. [[CrossRef](#)]
15. Xie, Z.; Lou, S.; Duan, Y.; Li, Z.; Chen, L.; Wang, H.; Zhang, Y.; Zhu, H. Passively Q-switched KTA cascaded Raman laser with 234 and 671 cm⁻¹ shifts. *Appl. Sci.* **2021**, *11*, 6895. [[CrossRef](#)]
16. Porto, S.P.S.; Scott, J.F. Raman spectra of CaWO₄, SrWO₄, CaMoO₄, and SrMoO₄. *Phys. Rev.* **1967**, *157*, 716–719. [[CrossRef](#)]
17. Frank, M.; Smetanin, S.N.; Jelínek, M.; Vyhlídal, D.; Ivleva, L.I.; Zverev, P.G.; Kubeček, V. Highly efficient picosecond all-solid-state Raman laser at 1179 and 1227 nm on single and combined Raman lines in a BaWO₄ crystal. *Opt. Lett.* **2018**, *43*, 2527–2530. [[CrossRef](#)]
18. Frank, M.; Smetanin, S.N.; Jelínek, M.; Vyhlídal, D.; Shukshin, V.E.; Ivleva, L.I.; Dunaeva, E.E.; Voronina, I.S.; Zverev, P.G.; Kubeček, V. Stimulated Raman scattering in alkali-earth tungstate and molybdate crystals at both stretching and bending Raman modes under synchronous picosecond pumping with multiple pulse shortening down to 1 ps. *Crystals* **2019**, *9*, 167. [[CrossRef](#)]
19. Frank, M.; Smetanin, S.N.; Jelínek, M.; Vyhlídal, D.; Shukshin, V.E.; Zverev, P.G.; Kubeček, V. Highly efficient, high-energy, picosecond, synchronously pumped Raman laser at 1171 and 1217 nm based on PbMoO₄ crystals with single and combined Raman shifts. *Opt. Express* **2020**, *28*, 39944–39955. [[CrossRef](#)]
20. Oeder, R.; Scharmann, A.; Schwabe, D.; Vitt, B. Growth and properties of PbWO₄ and Pb(WO₄)_{1-x}(MoO₄)_x mixed crystals. *J. Cryst. Growth* **1978**, *43*, 537–540. [[CrossRef](#)]
21. Efendiev, S.M.; Darvishov, N.G.; Nagiev, V.M.; Gasanly, N.M.; Gabrielyan, V.T.; Nikogosyan, N.S. Raman scattering in Pb(MoO₄)_{1-x}(WO₄)_x mixed crystals. *Phys. Stat. Sol.* **1982**, *110*, K21–K26. [[CrossRef](#)]
22. Nakamura, T.; Sugiyama, K.; Moriguchi, E.; Shoji, T. Synthesis of scheelite group minerals in the CaWO₄-CaMoO₄-PbMoO₄-PbWO₄ system from aqueous solutions at 100 °C. *Shigen-to-Sozai* **2002**, *118*, 217–221. [[CrossRef](#)]
23. Kuzmicheva, G.M.; Kaurova, I.A.; Brykovskiy, A.A.; Rybakov, V.B.; Gorobets, Y.N.; Shekhovstov, A.N.; Cousson, A. Structural investigation of Pb(Mo_xW_{1-x})O₄ solid solutions via X-ray and neutron diffraction. *Mater. Res. Bull.* **2016**, *78*, 134–140. [[CrossRef](#)]
24. Basiev, T.T.; Doroshenko, M.E.; Smetanin, S.N.; Jelínek, M.; Kubeček, V.; Jelínková, H.; Shekhovstov, A.N.; Kosmyna, M.B. Multi-wave SRS oscillation in PbMoO₄ and PbMo_{0.5}W_{0.5}O₄ crystals under 18 picosecond laser pumping. *Laser Phys. Lett.* **2012**, *9*, 853–857. [[CrossRef](#)]
25. Bloss, W.J.; Gravestock, T.J.; Heard, D.E.; Ingham, T.; Johnson, G.P.; Lee, J.D. Application of a compact all solid-state laser system to the in situ detection of atmospheric OH, HO₂, NO and IO by laser-induced fluorescence. *J. Environ. Monit.* **2003**, *5*, 21–28. [[CrossRef](#)] [[PubMed](#)]
26. Chuang, T.; Burns, P.; Walters, E.B.; Wysocki, T.; Deely, T.; Loose, A.; Lee, K.; Drumheller, B.; Schum, T.; Hart, M.; et al. Space-based, multi-wavelength solid-state lasers for NASA's Cloud Aerosol Transport System for International Space Station (CATS-ISS). *Proc. SPIE* **2013**, *8599*, 85990N.
27. Guo, R.; Akiyama, K.; Minamide, H.; Ito, H. All-solid-state, narrow linewidth, wavelength-agile terahertz-wave generator. *Appl. Phys. Lett.* **2006**, *88*, 091120. [[CrossRef](#)]
28. Frank, M.; Smetanin, S.N.; Jelínek, M.; Vyhlídal, D.; Shukshin, V.E.; Zverev, P.G.; Kubeček, V. Laser output radiation characteristics controlled by the GdVO₄ crystal length in the extracavity synchronously pumped Raman laser with combined Raman shift resulting in generation of 860 fs pulses at 1228 nm. In Proceedings of the OSA Laser Congress 2019- Paper JTh3A.32, Vienna, Austria, 29 September–3 October 2019.
29. Frank, M.; Smetanin, S.N.; Jelínek, M.; Vyhlídal, D.; Shukshin, V.E.; Ivleva, L.I.; Zverev, P.G.; Kubeček, V. Efficient synchronously-pumped all-solid-state Raman laser at 1178 and 1227 nm on stretching and bending anionic group vibrations in a SrWO₄ crystal with pulse shortening down to 1.4 ps. *Opt. Laser Technol.* **2019**, *119*, 105660. [[CrossRef](#)]
30. Baccaro, S.; Barone, L.M.; Borgia, B.; Castelli, F.; Cavallari, F.; Dafinei, I.; de Notaristefani, F.; Diamoz, M.; Fesinesi, A.; Leonardi, E.; et al. Ordinary and extraordinary complex refractive index of the lead tungstate (PbWO₄) crystal. *Nucl. Instr. Meth. A* **1997**, *385*, 209–214. [[CrossRef](#)]